Monthly Notices of the ROYAL ASTRONOMICAL SOCIETY

MNRAS **517,** 1058–1070 (2022) https://doi.org/10.1093/mnras/stac2658
Advance Access publication 2022 September 23

Stability of urea in astrophysical ices. A laboratory study of VUV irradiation and high-energy electron bombardment

Víctor J. Herrero,[1]★ Isabel Tanarro,[1] Izaskun Jiménez-Serra,[2] Héctor Carrascosa,[2] Guillermo M. Muñoz Caro[2] and Belén Maté[1]★

[1]*Instituto de Estructura de la Materia (IEM-CSIC), Serrano 121-123, E-28006 Madrid, Spain*
[2]*Centro de Astrobiología INTA-CSIC, Carretera de Ajalvir, km 4, Torrejón de Ardoz, E-28850 Madrid, Spain*

Accepted 2022 September 14. Received 2022 September 14; in original form 2022 April 26

ABSTRACT

The recent detection of urea in the interstellar medium raises questions about its stability in different astronomical environments. In this work, we have studied the stability of urea ices and urea/water ice mixtures under vacuum-ultraviolet (VUV; 6.3–10.9 eV) irradiation and high-energy (5 keV) electron bombardment at 30, 100, and 200 K. The evolution of the ices was monitored with infrared spectroscopy. CO_2, HNCO, and OCN^- were identified as reaction products in the 30 K samples. At the higher temperatures CO_2 and HNCO were hardly found in the processed ices. The measurements provided destruction cross-sections and allowed the derivation of radiation yields, G_{100}, and half-life doses for urea. G_{100} values were found to be low ($\approx$3.6–0.3 molecules/100 eV) both for VUV photons and high-energy electrons with electrons being slightly more efficient for the destruction of the molecule. These low G_{100} values are likely due to favourable mechanisms of energy dissipation or urea recombination. The stability of urea under irradiation increases with temperature which suggests that higher mobility improves the repair mechanisms. Estimates based on these laboratory data indicate that urea should be stable ($\approx 10^8$–10^9 yr) against irradiation in cold dense clouds and hot cores. It would not survive long ($\approx 10^3$–10^4 yr) on the bare surface of a Kuiper belt object, but would be well protected ($\approx 10^9$ yr) against radiation below a 30 μm ice layer. The high resistance of the molecule to radiation damage makes it a good candidate for prebiotic chemistry.

Key words: astrochemistry – molecular data – solid state: volatile – methods: laboratory: molecular – ISM: clouds – ISM: molecules.

1 INTRODUCTION

One of the most accepted theories to explain the emergence of replicative systems in the process of the origin of life is the primordial ribonucleic acid (RNA) world (Powner et al. 2009; Patel et al. 2015). This theory proposes that early forms of life may have used RNA alone for the storage and transfer of genetic information. RNA molecules are made up of four different nucleotides, which in turn consist of a nucleobase (i.e. a nitrogen heterocycle), a ribose, and a phosphate.

In several chemical schemes proposed to explain the formation of ribonucleotides, urea, and 2-aminooxazole stand as key precursors of nitrogen heterocycles and nucleobases such as pyrimidines, purines, hydantoins, and triazines (Powner et al. 2009; Menor-Salván & Marín-Yaseli 2012; Patel et al. 2015; Becker et al. 2019; Menor-Salván et al. 2020). Although these molecules could have been synthesized *in situ* under prebiotic conditions in an early Earth, it is believed that an important reservoir could also have come from outer space through the impact of interstellar dust particles and meteorites on Earth's surface (Chyba & Sagan 1992). Urea has indeed been found in meteorites such as Murchison and Orgueil (see e.g. Hayatsu et al. 1975; Cooper & Cronin 1995), and it has been discovered recently in interstellar space toward the Sgr B2 (N) massive star-forming region and the Galactic Centre giant molecular cloud G+0.693−0.027 (abundance of $\sim -1.5 \times 10^{-9}$ to 5×10^{-11}; Belloche et al. 2019; Jimenez-Serra et al. 2020). On the contrary, 2-aminooxazole has neither been found in meteorites nor in the interstellar medium (ISM) despite the fact that it has recently been searched for toward G+0.693−0.027 through a broad-band and a high-sensitivity spectral survey carried out toward this source (upper limit to its abundance of $\sim 8 \times 10^{-11}$; Jimenez-Serra et al. 2020).

By performing laboratory experiments on pure 2-aminooxazole ice and mixtures of 2-aminooxazole/H_2O, Maté et al. (2021) found that while this molecule could survive interstellar radiation [both ultraviolet (UV) photons and cosmic rays (CRs)] in molecular dark clouds for time-scales as long as 10^8 yr, it is expected to be destroyed efficiently on the surface of Kuiper belt objects (KBOs) in time-scales of a few 1000 yr. In addition, the stability of this molecule within the Solar system would be significantly reduced by its large absorption and photodecomposition at wavelengths larger than 200 nm. This makes 2-aminooxazole an unlikely organic compound to be present in meteorites and small asteroids.

In contrast to 2-aminooxazole, little is known about the resistance and survivability of urea under interstellar irradiation with UV photons and CRs. The UV photolysis and radiolysis of different forms of urea have been investigated by various groups. Experimental

★ E-mail: v.herrero@csic.es (VH); belen.mate@csic.es (BM)

data are available for crystalline solids (Renoult et al. 1969; Poch et al. 2014), aqueous solutions (Navarro-González, Negrón-Mendoza & Chacón 1989; Terasaki et al. 2002), and isolated molecules in noble gas matrices (Duvernay et al. 2005). At room temperature, urea was found to be highly stable under γ-ray irradiation, both in water solution and in crystalline form (Renoult et al. 1969; Navarro-González et al. 1989), and the molecule in aqueous solution is also very resistant to UV (172 nm) photochemical decomposition (Terasaki et al. 2002). It is assumed that efficient mechanisms for energy dissipation from the initially excited states or for the reformation of urea from the initial fragments are responsible for these results. However, it is not known how effective these mechanisms will be under the conditions of interstellar icy grain mantles that are the presumed reservoirs of urea in the ISM.

In this work, we present an experimental investigation of the interaction of urea and urea/water ices with vacuum-ultraviolet (VUV) photons from a D_2 lamp and with 5 keV electrons, which simulate the secondary UV field in cold dense clouds and the effects of the secondary electrons produced by CRs on the ices, respectively (Kaiser et al. 2013; Cruz-Díaz et al. 2014; Mason et al. 2014; Maté et al., 2015, 2016, 2018). The experiments are carried out for ice temperatures of 30, 100, and 200 K, which are relevant for ice mantles in cold clouds and outer Solar system bodies, and also for hot cores. The evolution of the ice samples under energetic processing is monitored by infrared (IR) spectroscopy, which allows the identification of newly formed products and the derivation of destruction cross-sections for urea. The energy doses required for the destruction of a given amount of urea are used for the estimate of its survival probability in interstellar and cometary ices.

2 EXPERIMENTAL SECTION

The experiments were carried out in a high vacuum (HV) set-up described in previous works (Maté et al., 2014, 2021; Timón et al. 2021). The background pressure in the chamber, P_b, was in the 10^{-8} mbar range. Urea (99 per cent Merck) was evaporated from a copper oven (Maté et al. 2011), whose inner wall was covered with a stainless steel foil (Maté et al. 2021), at $T = 70$–90^{o}C and was deposited on an IR transparent substrate. Discs of silicon and KBr were tried as substrates. No appreciable differences were found in the results on the two substrates, and Si was chosen for most experiments to avoid possible problems with the hygroscopic KBr for water containing ices. Typical deposition times were usually tens of seconds. The substrates were fitted to a Cu holder in contact with the cold head of a He compression cryostat (Maté et al. 2021). Deposition temperatures were in the 30–200 K range. Mixtures of urea with water were also studied. To this end, vapours of water and urea were simultaneously deposited on the substrate. Water vapour was introduced through a leak valve and was allowed to backfill the chamber. A mixture of water and urea was deposited on the face of the substrate in front of the urea evaporation oven, which was then processed. A layer of just water, formed from background vapour deposition on the opposite side of the substrate, remained unprocessed and had to be discounted in the analysis of the data (see below). The deposited urea ice samples and their evolution with processing time were monitored with IR spectroscopy. After deposition, the samples were rotated to intercept at right angles the beam of a (Bruker Vertex70) Fourier transform infrared spectrometer (FTIR) traversing the chamber.

UV irradiation of the urea samples was carried out with a Hamamatsu L10706 deuterium (D_2) lamp (Maté et al. 2018) whose emission was largely concentrated in the 120–180 nm range. For this wavelength interval, the photon flux on the sample was estimated to be $\varphi_0 = 7.5 \times 10^{13}$ photons cm^{-2} s^{-1}, from the data provided by the manufacturer.

Electron irradiation was performed with the electron gun described in previous works (Maté et al. 2014, 2015, 2016). The electron energy was fixed at 5 keV. Two values of the electron flux falling on the sample were tried: $\varphi_e = 4 \times 10^{12}$ and 2×10^{12} electrons cm^{-2} s^{-1}. The results with the two flux values were checked to be consistent and they were used indistinctly.

For the processing of the ice samples, the side of the substrate containing the urea deposits was made to face the UV lamp or the electron beam. In the course of processing, the substrate was rotated, at selected time intervals, to record an IR spectrum. Typical processing times were between 30 and 60 min.

2.1 VUV absorption spectrum

The vacuum-ultraviolet (VUV) absorption of urea was measured at the Interstellar Astrochemistry Chamber (ISAC), described in Muñoz Caro et al. (2010). Basically, ISAC consists of an ultra-high-vacuum (UHV) chamber, with pressure typically in the range $P = 3$–4×10^{-11} mbar, where an ice layer is deposited at 8 K. The urea sample was characterized by transmittance FTIR spectroscopy and VUV spectroscopy. The source used for VUV spectroscopy is an F-type microwave-discharge hydrogen flow lamp (MDHL), from Opthos Instruments, with a VUV flux of 2.5×10^{14} cm^{-2} s^{-1} at the normal sample position measured with a calibrated Ni mesh.

The VUV spectrum was measured using a McPherson 0.2 m focal length VUV monochromator (model 234/302) with a photomultiplier tube (PMT) detector equipped with a sodium salicylate window, with a resolution of 0.2 nm (see Cruz-Díaz et al. 2014 for details).

The main emission bands are Lyα at 121.6 nm (10.20 eV) and the molecular hydrogen bands around 157.8 nm (7.85 eV) and 160.8 nm (7.71 eV) for the operating hydrogen pressure of 0.4 mbar. The interface between the MDHL and the vacuum chamber is an MgF_2 window. The monochromator is located at the rear end of the ISAC chamber, separated by another MgF_2 window. Because of its high volatility under vacuum, the urea sample was not placed inside the ISAC chamber, instead it was located close to the entrance slit of the VUV monochromator, pumped up by a turbo molecular pump. The background VUV spectrum corresponding to the MDHL emission was subtracted from the one with the urea sample. A solution of urea in ethanol was used for the preparation of the sample. A drop of this solution was placed on the substrate and a deposit of polycrystalline urea was obtained after evaporation of the ethanol. Unfortunately, the solid deposit thus obtained was irregular and it was not possible to derive reliable column densities for the direct determination of the absolute absorption cross-section. The absorption cross-sections were estimated indirectly by scaling the measured spectrum to the absorption coefficients obtained by Campbell & Clark (1989) from reflection spectra performed on urea monocrystals (see below).

3 RESULTS

3.1 Deposited samples

Urea and urea/water ice samples were deposited at substrate temperatures between 30 and 200 K. Polycrystalline urea was formed at 200 K. The rest of the ices were amorphous. The fresh deposited samples were characterized by their IR transmission (absorbance) spectra. Typical spectra are shown in Fig. 1. Spectral assignments and band strengths of the absorption features in the 3800–1100 cm^{-1}

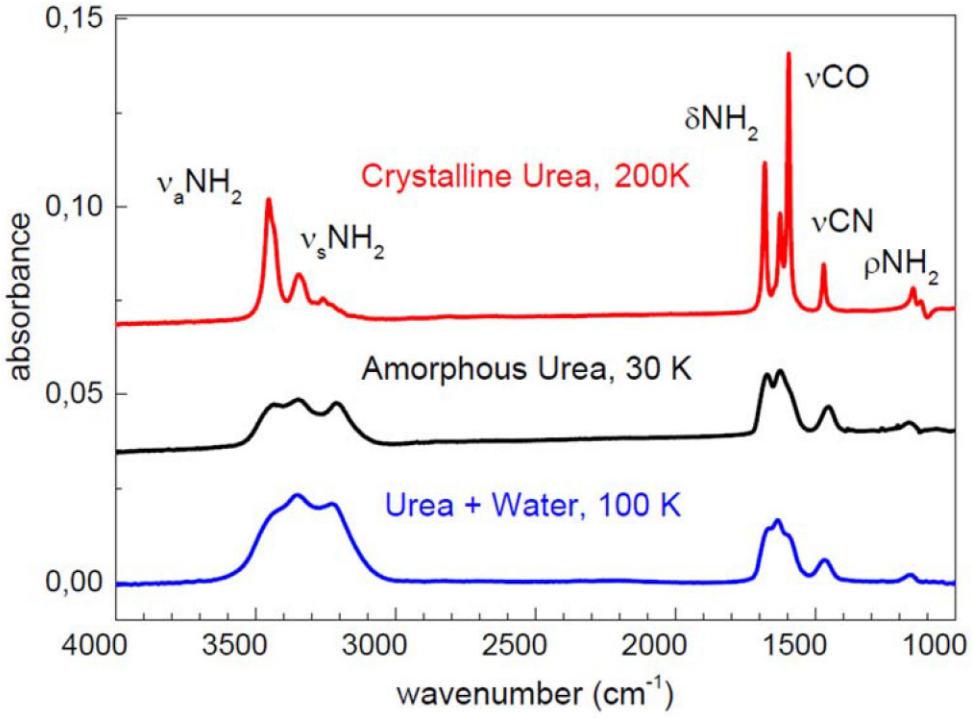

Figure 1. IR spectra (4000–1000 cm^{-1}) of typical samples as deposited. Black trace: pure amorphous urea at 30 K. Red trace: crystalline urea deposited at 200 K. Blue trace: urea (58 per cent)/water mixture, deposited at 100 K. They correspond to samples E1, E2, and E4 of Table 1.

interval are given in Timón et al. (2021). The column densities of the deposited urea samples were estimated from

$$N = 2.303 \times \frac{\int \mathrm{Abs}\,(\nu)\ \mathrm{d}\nu}{A}, \quad (1)$$

where Abs(ν) denotes the frequency-dependent IR absorbance of a given band and A the corresponding band strength. We have taken in all cases the band at 1521–1390 cm^{-1} (νCN) and have used the band strength $A_{\nu\mathrm{CN}} = 1.25 \times 10^{-17}$ cm molecule^{-1} for amorphous samples, between 30 and 140 K, and the band strength $A_{\nu\mathrm{CN}} = 1.6 \times 10^{-17}$ cm molecule^{-1} for crystalline samples at 200 K. This band is comparatively weak, but the most intense absorption features in the spectral interval of interest that are found at 3710–3021 cm^{-1} (νNH) and at 1770–1520 cm^{-1} (δNH_2, νCO) coincide with absorptions of water and are problematic for experiments with water mixtures. For consistency, we have used the νCN band for the calculation of urea column densities in all the experimental samples.

For the estimates of the amount of water in the mixtures to be processed, it is necessary to take into account that water ice is deposited from the background vapour on the two sides of the substrate, whereas urea is deposited from the evaporation oven just on one side. The energetic processing experiments are restricted to the face of the substrate containing the mixture of water and urea, and consequently the spectrum of pure water ice from the unprocessed side of the substrate must be discounted. To do so, we have used the intense νOH band at 3000 cm^{-1}. The following correction has been applied to the measured band intensities (integrated absorbances):

$$I_{\mathrm{corr}}(\nu\mathrm{OH}) = I(\nu\mathrm{OH} + \nu\mathrm{NH}) - 10 \times I(\nu\mathrm{CN}) - (I(\nu\mathrm{OH} + \nu\mathrm{NH}) - 10 \times I(\nu\mathrm{CN}))/2, \quad (2)$$

where $I_{\mathrm{corr}}(\nu\mathrm{OH})$ represents the corrected νOH band intensity of water ice (i.e. that relevant for the processing experiments). The first term on the right-hand side, $I(\nu\mathrm{OH} + \nu\mathrm{NH})$, corresponds to the measured signal and includes all contributions in the path of the IR beam. Note that in this wavelength region there is also a contribution from the νNH band of urea. The second term discounts this νNH contribution, which is estimated to be approximately $10 \times I(\nu\mathrm{CN})$ from the spectra of pure urea. The third term discounts the contribution of water ice in the unprocessed side of the substrate. The column densities of water were calculated with equation (1) using the $\int_{\mathrm{corr}}(\nu\mathrm{OH})$ values given by equation (2) and the band strengths of Mastrapa et al. (2009) for the νOH band of water ($A_{\nu\mathrm{OH}} = 1.9 \times 10^{-16}$ at $T = 30$ K, $A_{\nu\mathrm{OH}} = 3 \times 10^{-16}$ cm molecule^{-1} at 100 K, and $A_{\nu\mathrm{OH}} = 2.7 \times 10^{-16}$ cm molecule^{-1} at 140 K). The column densities of urea and water used in the processing experiments are listed in Table 1. Uncertainties in the column densities are given in the table caption. They are mostly due to the uncertainties in the band strengths (Timón et al. 2021).

The selected ice layers are thin (less than 100 nm). This is appropriate for the observation of the destruction of urea upon processing, which is the main objective of this study, but renders difficult the observation of minor photolysis products.

3.2 Reaction products

In the course of energetic processing, both with UV photons and with high-energy electrons, the IR spectra of the samples are transformed. In the 3900–3100 cm^{-1} range, the destruction of the NH bonds leads to a decrease of the corresponding NH stretching band, but signals in this region can be perturbed by the strong OH absorption band (1.9–3 $\times 10^{-16}$ cm molecule^{-1}) of background water that can deposit on both sides of the substrate during the experiments and we have not used these data in our analysis. Unless otherwise stated, we have also neglected the region below 1200 cm^{-1} including the ρNH_2 band (1195–1141 cm^{-1}) because the measurements in this region were often affected by spurious peaks, due to absorptions

Table 1. Ice samples used in the processing experiments. N_u and N_w correspond to the column densities of urea and water, respectively, ρ is the volume density of the ice, and h the estimated sample thickness. The densities of the pure urea ices are taken from Timón et al. (2021), and the temperature-dependent density of amorphous water has been taken from Dohnhálek et al. (2003). The density of the mixtures has been approximated as $\rho \approx f_1\ \rho_1 + f_2\ \rho_2$, where f_i is the molecular fraction of component i. The sample thickness was calculated as the quotient (in appropriate units) between the column density and the volume density. The samples labelled 'VUV' correspond to photon irradiation with the D_2 lamp (see text) and those labelled 'E' to bombardment with 5 keV electrons. Estimated uncertainties are ≈40 per cent for N_u, ≈20 per cent for N_w, and ≈30–40 per cent for h.

Sample	T (K)	N_u (molecules cm^{-2})	N_w (molecules cm^{-2})	ρ (g cm^{-3})	h (nm)
VUV1: urea, amorphous	30	5.4×10^{16}	–	1.38	31
VUV2: urea, amorphous	100	6.7×10^{16}	–	1.38	49
VUV3: urea, crystalline	200	7.1×10^{15}	–	1.32	5.4
VUV4: urea (47 per cent)/water	30	3.7×10^{16}	4.2×10^{16}	0.99	44
VUV5: urea (31 per cent)/water	140	3.8×10^{16}	8.6×10^{16}	1.04	54
E1: urea, amorphous	30	7.0×10^{16}	–	1.38	42
E2: urea, amorphous	100	8.5×10^{16}	–	1.38	50
E3: urea, crystalline	200	4.3×10^{16}	–	1.32	22
E4: urea (58 per cent)/water	30	4.2×10^{16}	3.1×10^{16}	1.07	48
E5: urea (23 per cent)/water	100	4.2×10^{16}	1.4×10^{17}	0.93	85

of the (doped) Si substrate, which were found to be sensitive to slight temperature changes or to the effects of the processing agents. Therefore, we have concentrated in the 2500–1200 cm^{-1} range. The main transformations observed in this range, which are attributed to the destruction of part of the original urea and to the possible formation of new products, are described in Table 2 and shown in Fig. 2.

In the coldest (30 K) samples investigated, three bands attributed to CO_2, HNCO, and OCN^- (Lowenthal, Kahnna & Moore 2002; Maté et al. 2018) are always found, irrespective of the type of ice (pure urea or urea/water mixture) and of the processing agent (VUV photons or high-energy electrons). In all the higher temperature ices (100–200 K), OCN^- is by far the dominant product and only very small amounts of CO_2 and HNCO are found in some of the samples, with one exception; in the photolysis of crystalline urea a peak also appears at 1365 cm^{-1} that we have not been able to assign. The virtual absence of CO_2 and HNCO peaks in the processed samples of higher temperature ices can be due to a change in the prevailing dissociation routes or to desorption of these volatile molecules. Fig. 2 is only illustrative of the type of products formed in each case, and although at first sight it might seem that electron bombardment leads to a larger product formation and thus, to a larger destruction of urea, a proper quantitative analysis requires consideration of the energy doses imparted to the various samples. This is done in Section 3.3.3. The appearance of the same products in photolysis and radiolysis, despite the different mechanisms implied in principle in the two processes, is a common finding in the processing of organic molecules in astrophysical ice analogues (see e.g. Arumainayagam et al. 2019).

Besides CO_2, HNCO, and OCN^-, which are clearly identified by the appearance of characteristic peaks in a spectral interval free from other absorptions, we surmise that other products may be formed, with absorption bands in the same spectral regions as those of urea. In previous works on the photolysis and radiolysis of urea, a wide variety of products were observed. In the UV photolysis ($\lambda > 160$ nm) of urea in Ar and Xe matrices (10–30 K), Duvernay et al. (2005) reported the observation of CO, hydrazine (N_2H_4), NH_3, HNCO, cyanamide (H_2NCN), H_2O, and isourea ($H_2N(OH)C=NH_2$). The cold, inert environment around the isolated urea molecules is ideal for the identification of primary dissociation pathways, but is very different from the ices of our study. In a simulation of the effects of UV radiation on the surface of Mars, Poch et al. (2014) studied the UV photolysis ($\lambda = 200$–250 nm) of crystalline urea at $T = 218$ K. These authors used IR spectroscopy and found only OCN^- and NH_4^+ as photoproducts. No polymerization products were detected. In the γ-ray radiolysis of room temperature crystalline urea, Renoult et al. (1969) found the following products: H_2, N_2, NH_3, hydroxylamine (H_2NOH), formamide (H_2NCHO), oxamide (H_2N-CO-CO-NH_2), semicarbazide (H_2N-CO-NH-NH_2), biuret (H_2N-CO-NH-CO-NH_2), and biurea (H_2N-CO-NH-NH-CO-NH_2). For the product analysis, these authors used mostly spectrophotometric, chromatographic (GC), and mass spectrometric (MS) techniques. Navarro-González et al. (1989) investigated the γ-ray radiolysis of room temperature aqueous solutions of urea. Using also GC–MS techniques they observed in the irradiated samples the presence of H_2, CO_2, NH_3, oxalic acid (HOOC-COOH), malonic acid (HCOOC-CH_2-COOH), and three unidentified oligomers, possibly polyureas, with molecular weight higher than 1000.

It is likely that some of these products are also formed in our experiments, but except for CO_2, HNCO, and NCO^-, they cannot be unequivocally identified with IR spectroscopy alone. Some of them have the same functional groups as urea and their IR spectra present absorptions in the same spectral regions, albeit with different band shapes and intensities. They could contribute somehow to the changes, both in shape and intensity, observed in the absorption bands during processing and thus introduce uncertainty, but by analogy with the literature results just mentioned (Renoult et al. 1969; Navarro-González et al. 1989; Duvernay et al. 2005; Poch et al. 2014) we expect that the prevalent dissociation channels will lead to small molecules that will not interfere much with the absorptions of urea. It is worth noting that urea fits in an isoelectronic sequence with carbonic acid and acetone: $O=C(OH)_2$, $O=C(NH_2)_2$, and $O=C(CH_3)_2$. Under energetic processing, carbonic acid ice has been shown to decompose into H_2O and CO_2 (Peeters et al. 2010), and acetone ice into CH_4 and H_2C_2O (ketene) among other products (Hudson 2018). In a similar way, urea, the middle term in the sequence, should decompose into NH_3 and HNCO. Acid base reactions could transform HNCO and NH_3 into OCN^- and NH_4^+. As indicated repeatedly in the text, HNCO and OCN^- were found in our measurements, but we did not find NH_3 (expected peak

Table 2. Main qualitative transformations observed during the energetic processing of pure urea and urea mixed with water.

Spectral range (cm^{-1})	VUV and 5 kV electron processing	Observations
2353–2331	Appearance of a band and growth in samples at $T = 30$ K	Formation of CO_2
2285–2215	Appearance of a band and growth in samples at $T = 30$ K	Formation of HNCO
2200–2125	Appearance of a band and growth in all samples	Formation of OCN^-
1770–1520	Band decrease in most samples with some exceptions (see Figs 4 and 5). Modification of the band profile, especially in warm ($T = 100$ K) samples	Destruction of CO, NH bonds. Possible changes in the ice morphology or product formation
1520–1390	Band decrease in 30 K samples and in crystalline samples (200 K). In amorphous samples at $T = 100$ K band slightly blueshifted (≈8 cm^{-1})	Destruction of CN bonds. Possible changes in the ice morphology or product formation

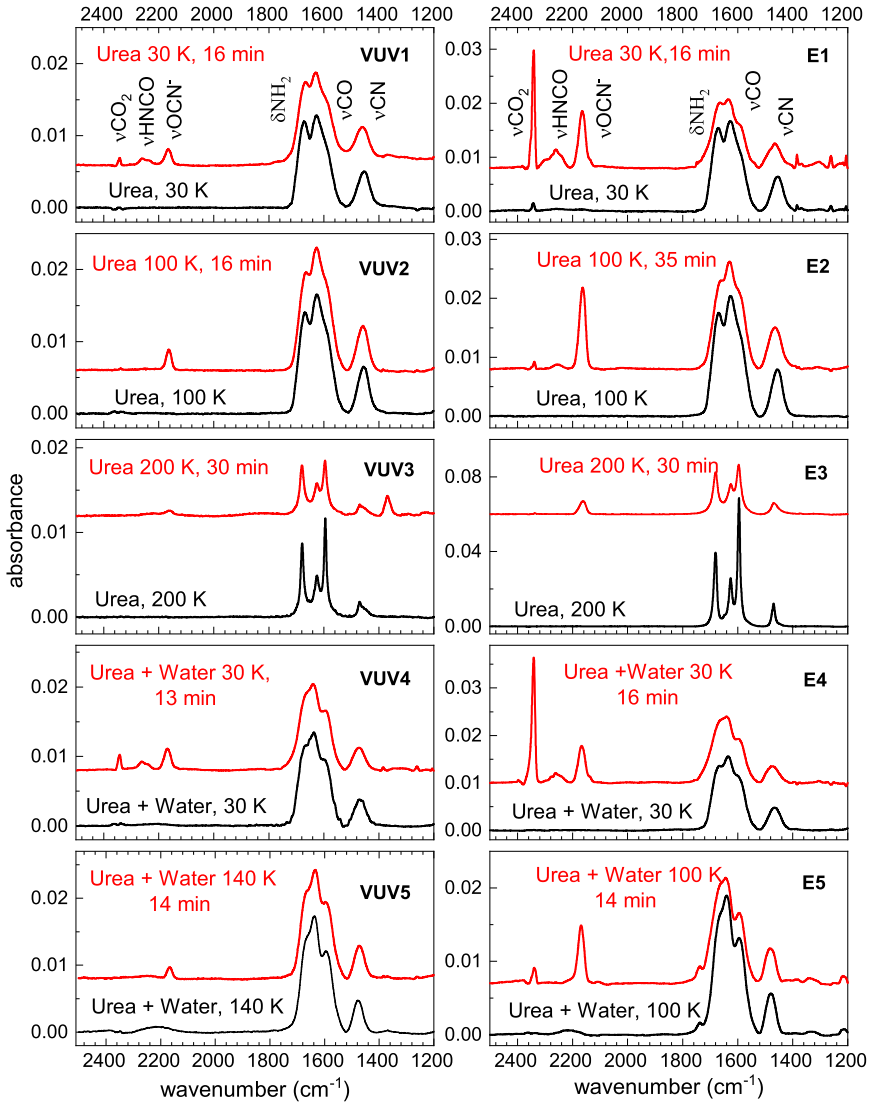

Figure 2. Evolution of the 2500–1200 cm^{-1} IR spectra of urea and urea/H_2O mixtures under VUV irradiation (left-hand column) and high-energy (5 keV) electron bombardment (right-hand column). Black traces: fresh deposited samples; red traces: processed samples. The labels VUV1–VUV5 and E1–E5 correspond to the samples listed in Table 1.

at 1070 cm^{-1}, $A = 1.4 \times 10^{-17}$ cm molecule^{-1}). The presence of NH_4^+, which has been reported by Poch et al (2014) in the photolysis of crystalline urea, is not evident in our measurements, but cannot be completely excluded. The ν_4 bending mode of ammonium ($A = 4.1 \times 10^{-17}$ cm molecule^{-1}; van Broekuizen et al. 2004) appears at 1440–1480 cm^{-1}, but its exact location and bandwidth are strongly dependent on the ice environment (see discussion in Maté et al. 2009; Gálvez et al. 2010). In our case, the corresponding ammonium band, which would be the most obvious counterion for OCN^-, could be masked by the νCN band of urea. Compounds of very high molecular weight do not seem to form in appreciable amounts in our experiments, since all products evaporate without leaving any residue upon warming of the substrate to 300 K during a few minutes.

3.3 Kinetics

Under irradiation with VUV photons or high-energy electrons, urea is expected to undergo initially a first-order decomposition process characterized by a destruction cross-section, $\sigma_{\rm des}$:

$$N(t) = N_0\,{\rm e}^{-kt} = N_0\,{\rm e}^{-\sigma_{\rm des}F}, \quad (3)$$

where N represents the concentration of urea and F is the fluence, which is usually expressed in photons or electrons cm^{-2}. The concentration of urea at a given time is proportional to the intensity of the absorption bands (absorbance), and equation (3) can be transformed into

$$\ln\frac{I_F}{I_0} = -\sigma_{\rm des}F, \quad (4)$$

where I_0 and I_F represent the initial intensity and the intensity at fluence F. As irradiation proceeds, the structure of the sample might change and the products formed can induce secondary reactions leading to a deviation from the linear behaviour expressed by equation (4). In any case, we will assume that this equation describes always the band intensity decay at least at the start of energetic processing. It is possible that the various absorption bands lead to different destruction cross-sections, since they correspond to different molecular vibrations and involve different bonds. As indicated above, in this study we have focused on the evolution of bands at 1770–1520 cm^{-1} (δNH$_2$ + νCO) and 1521–1390 cm^{-1} (νCN). Note that the data from the δNH$_2$ + νCO band are more problematic, since they can be perturbed by contributions from water and from possible photolysis/radiolysis products.

3.3.1 VUV photolysis

VUV absorption is usually large in ices. This can lead to a significant attenuation of the initial photon flux, φ_0, during the passage of the light beam through the laboratory samples, which in general will not be optically thin. Equation (4) is still valid at the beginning of the irradiation process, but, in order to account for the flux attenuation, an average photon flux, $\varphi_{\rm av}$, in the sample must be used for the calculation of the fluence (Maté et al. 2021):

$$\phi_{\rm av} = -\frac{\phi_0}{N_0\sigma_{\rm a}}\left({\rm e}^{-\sigma_{\rm a}N_0} - 1\right), \quad (5)$$

where $\sigma_{\rm a}$ is the VUV absorption cross-section. The fluence in equation (4) is now calculated as $F = \varphi_{\rm av}\,\Delta t$, where Δt is the processing time.

The VUV absorption spectrum of room temperature polycrystalline urea, measured at the ISAC set-up (Muñoz-Caro et al. 2010), is shown in Fig. 3. As indicated above, the absolute values of the cross-section were obtained from a scaling of this spectrum to the results of Campbell & Clark (1989). These authors determined absorption coefficients through Kramers–Kronig analysis of polarized reflection spectra of single crystals of urea. The isotropic absorption spectrum derived from their measurements is in qualitative agreement with that of this work, that shows a decay with growing energy between 165 and 145–135 nm and then a smaller increase towards 130 nm. Our spectrum is scaled so that the average cross-section coincides with that from the data of Campbell & Clark (1989) for the measured wavelength interval. The data of Campbell & Clark extend to larger wavelengths and show a marked decrease in the absorption for $\lambda >$ 165 nm. For the kinetic analysis of this section we do not consider the wavelength dependence and use simply the average value of the cross-section, $\sigma_{\rm a}$(urea) $\approx 2.8 \times 10^{-17}$ cm^2, over the wavelength range of the D$_2$ lamp. For binary mixtures we have further assumed

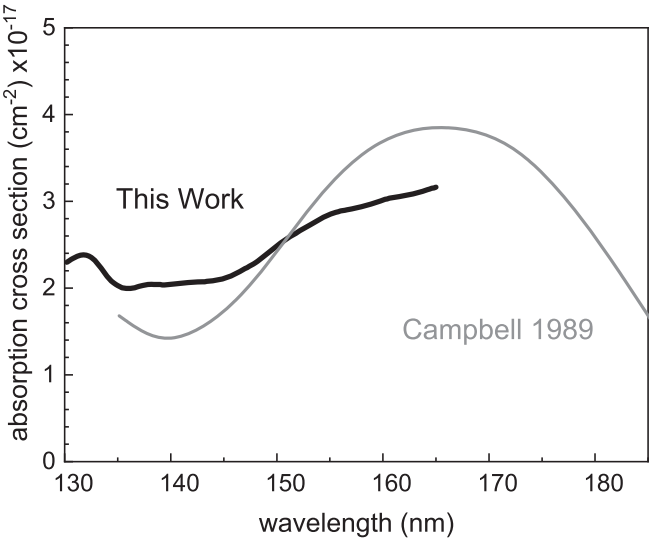

Figure 3. VUV absorption cross-section of room temperature crystalline urea. Grey curve: adapted from the single crystal data of Campbell & Clark (1989). Black trace: absorption spectrum of polycrystalline urea from this work scaled to the absolute values of Campbell & Clark over the common wavelength interval (see the text).

$\sigma_{\rm a} \approx f_1\sigma_{\rm a1} + f_2\sigma_{\rm a2}$, where indices 1 and 2 correspond to the two mixture components and f_i is the relative fraction of each component. The average absorption cross-section of water ice over the 120–180 nm range, $\sigma_{\rm a}({\rm H_2O}) \approx 3 \times 10^{18}$ cm^2, was taken from Cruz-Díaz et al. (2014).

The photolysis experiments were carried out at 30 and 100 K for pure amorphous urea, at 200 K for crystalline urea, and at 30 and 140 K for mixtures of urea and water. As indicated above, three new bands, corresponding to νCO$_2$, νHNCO, and νOCN$^-$, appear in the 2400–2000 cm^{-1} interval (see Table 2). These bands grow with processing time. The CO$_2$ band presents a high variation between experiments and it is possibly contaminated by CO$_2$ background deposition. Both CO$_2$ and HNCO disappear almost completely in the experiments at $T \geq 100$ K. The OCN$^-$ band shows a monotonic growth with time in all the experiments (cold and warm, amorphous and crystalline, and pure urea and mixtures) and it provides a lower limit for the destruction of urea. Taking a band strength of $A = 1.3 \times 10^{-16}$ cm molecule^{-1} (van Broekhuizen et al. 2004), the amount of OCN$^-$ formed in the various experiments corresponds to a destruction of a few per cent in the initial urea molecules. It is a small variation as compared with the decays of the δNH$_2$ + νCO and νCN bands, but the growth of the νOCN$^-$ band is observable even in the few experiments where no clear decay is seen within the scatter of the data of the δNH$_2$ + νCO and νCN bands.

The evolution of the δNH$_2$ + νCO (1772–1520 cm^{-1}) and νCN (1521–1390 cm^{-1}) bands under VUV irradiation was monitored over time and is displayed in Fig. 4. In the coldest (30 K) samples (VUV1, VUV4), the two bands decay with irradiation. The decay is faster for the νCN band, which suggests that the CN bonds are more easily broken than the C = O bonds. An approximately exponential decay, consistent with equation (4), is observed for the first 8–10 min. A fit of the measured data to equation (4) is shown in the right-hand column of Fig. 4, and the corresponding destruction cross-sections are listed in Table 3. The 30 K destruction cross-sections for pure urea and urea mixed with water are similar. This good coincidence suggests that water ice plays no drastic role in the destruction of urea. The radicals formed in the photolysis of H$_2$O could recombine

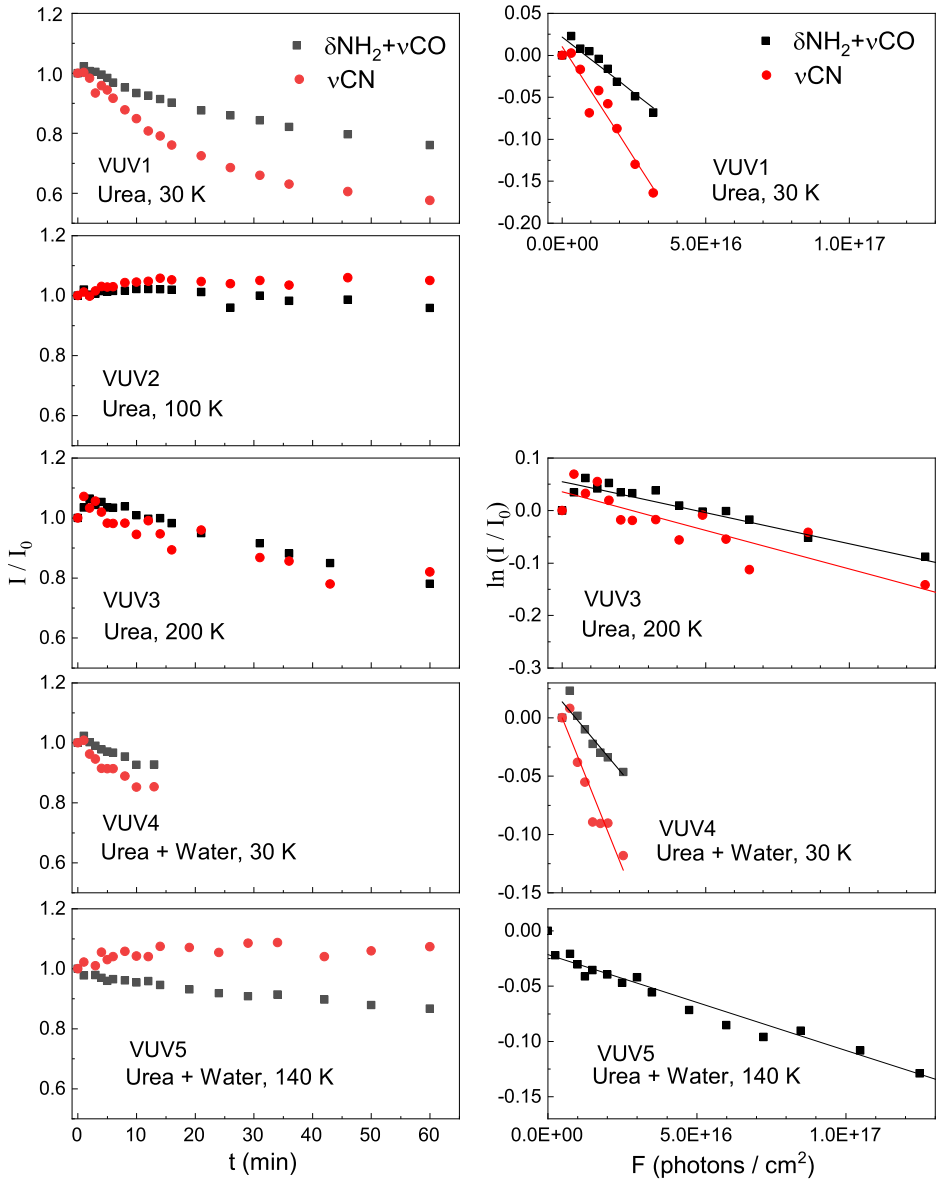

Figure 4. Evolution of the $\delta NH_2 + \nu CO$ (black squares) and νCN (red circles) bands of urea under VUV (120–180 nm) photolysis. The labels VUV1–VUV5 correspond to the samples of Table 1. Left-hand column: evolution of the band intensities normalized to the initial value (I/I_0) as a function of time. Right-hand column: fit (straight lines) of the linear decay interval in $\ln(I/I_0)$ to equation (4). The missing panel in this column corresponds to VUV2, where no band decay was observed. The cross-sections derived from the fit are listed in Table 3.

again to water molecules within the solid. Water ice would thus act primarily as a shield absorbing part of the incident radiation and its effect would be mostly felt as a decrease of φ_{av}, but would not much change the value of σ_{des}. A similar result was obtained in a previous work by our group on the photolysis of 2-aminooxazole (Mate et al. 2021). This suggestion should be taken with care, since the present data do not allow a firm conclusion on the effect of water. This would require the performance of experiments with a much higher urea dilution, which are technically difficult. Besides, there is a large uncertainty (30–40 per cent) in the cross-section values.

Within the data dispersion, no decay is observed in any of the two bands of the warm (100 K) sample of amorphous urea (VUV2), and therefore no fit is presented in the right-hand column of Fig. 4. In fact, a slight growth of νCN followed by stabilization can be seen. Possibly at this temperature the much higher mobility within the amorphous solid and an efficient cage effect facilitate the fast reformation of urea. Other possibilities, which are deemed less likely, would be an appreciable change in the band strengths with temperature, and the formation of a great amount of products with similar absorption bands that compensate or even reverse the decrease due to the disappearance of urea. Some destruction of urea can be deduced from the growth of the νOCN^- band (see above). At the end of the experiment (60 min, $F = 1.4 \times 10^{17}$ photons cm^{-2}) 3×10^{15} OCN^- ions cm^{-2} are formed. This corresponds to a destruction of about 4 per cent of the initial urea. Considering that each OCN^- anion comes from one molecule of urea, one can take the rate for OCN^- production as a lower limit for the rate of urea destruction. From the approximately linear growth of OCN^- during the first 16 min (not shown for brevity), the lower limit for urea destruction cross-section is $\sigma_{des} \approx 4 \times 10^{-19}$ cm^2. A somewhat similar behaviour is observed in the warm (140 K)

Table 3. VUV photolysis of urea ices and urea/water ices. Uncertainties (in per cent) are estimated with numerical checks and error propagation in the formulas used to calculate the various quantities in the table. φ_{av}, average photon flux (±25 per cent, equation 5); f_u, molecular fraction of urea (±30 per cent); σ_{des}, destruction cross-section (±30 per cent for pure urea, ±40 per cent for mixtures, fit to equation 4); $D_{1/2}$, half-life dose (±25 per cent for pure urea, ±50 per cent for mixtures, equations 9 and 10); G_{100}, radiation yield (±20 per cent for pure urea, ±30 per cent for mixtures, equations 13 and 14); Φ_p, photon yield (±30 per cent for pure urea, ±50 per cent for mixtures, equations 15 and 16).

Sample	φ_{av} $\times 10^{13}$ photons cm^{-2} s^{-1}	σ_{des} $\delta NH_2 + \nu CO$ $\times 10^{-18}$ cm^2	σ_{des} νCN $\times 10^{-18}$ cm^2	$D_{1/2}$ $\delta NH_2 + \nu CO$ eV $molecule^{-1}$	$D_{1/2}$ νCN eV $molecule^{-1}$	G_{100} $\delta NH_2 + \nu CO$ molecules 100 eV^{-1}	G_{100} νCN molecules 100 eV^{-1}	Φ_p $\delta NH_2 + \nu CO$ $molecules\ photon^{-1}$	Φ_p νCN $molecules\ photon^{-1}$
VUV1 Urea am. $T = 30$ K	4.3	3.3	6.5	47	24	1.4	2.9	0.12	0.23
VUV2[a] Urea am.	3.4	(0.4)	(0.4)	(393)	(393)	(0.2)	(0.2)	(0.01)	(0.01)
$T = 100$ K									
VUV3 Urea cry.	6.6	1.2	1.5	131	105	0.5	0.7	0.04	0.02
$T = 200$ K									
VUV4 Urea/H_2O	3.7	2.9	6.1	61	29	1.1	2.4	0.09	0.19
$f_u = 0.47$ $T = 30$ K									
VUV5 Urea/H_2O	3.8	0.9	–	224	–	0.31	–	0.02	–
$f_u = 0.31$ $T = 140$									

[a]From the growth of OCN^-, a lower limit of $\sigma_{des} \approx 4 \times 10^{-19}$ cm^2 can be estimated for the global destruction of pure urea at 100 K (see the text). This cross-section value and the corresponding energetic yields are represented in parentheses.

urea/water mixture (VUV5). The νCN band grows slightly at the start and then stabilizes. In this case, however, the $\delta NH_2 + \nu CO$ band does decrease, although at a slower pace than that observed for the cold samples.

In the VUV irradiation of crystalline urea both bands grow slightly at the beginning, pointing to a possible rearrangement of the sample, and then decrease linearly with growing time. In the crystalline solid, the linear decay of $\ln(I/I_0)$ extends for at least 30 min, with F in the 10^{17} photons cm^{-2} range, but the dispersion in the data for the νCN band is very large. The destruction cross-sections are appreciably smaller than those for cold (30 K) amorphous urea, indicating that urea is comparatively stable against VUV radiation within the crystal structure with a strong tridimensional hydrogen bonding network. The destruction cross-sections for the warm amorphous samples are even smaller than those for the crystalline ice due possibly to the rapid reformation of urea prompted by a higher mobility of the photofragments and an efficient cage effect.

3.3.2 *High-energy electron bombardment*

The evolution of the $\delta NH_2 + \nu CO$ and νCN bands of pure urea in the samples subjected to bombardment by 5 keV electrons is shown in Fig. 5. In the pure urea samples, the behaviour of these bands in the course of processing has some qualitative similitudes with that of VUV photolysis: the decay in the band intensities is slower for the samples at $T \geq 100$ K (E2, E3) than for that at $T = 30$ K, and for this sample (E1) the initial decay of the νCN band is faster than that of $\delta NH_2 + \nu CO$. With progressing electron bombardment, the decay of the bands in the E1 sample tends to stabilize and the $\delta NH_2 + \nu CO$ and νCN curves cross after 12 min of irradiation, which corresponds to a fluence of 2.9×10^{17} electrons cm^{-2}. Such a crossing was not observed in the photolysis experiments (Fig. 4). In the crystalline sample (E3), the $\delta NH_2 + \nu CO$ band decays faster that νCN band, in contrast with the behaviour observed in photolysis (VUV3 sample), where the two bands were found to decrease at a similar rate. In the mixed urea/water ices irradiated with electrons (E4, E5), the two bands show a sharper initial decay than their photolysis counterparts (Fig. 4, samples VUV4 and VUV5), and then tend to stabilize or even grow for long bombardment times.

A fit of the normalized band intensities to equation (4) is shown in the right-hand column of Fig. 5 for the various urea samples investigated. The corresponding destruction cross-sections are listed in Table 4. For the cold (30 K) sample of pure urea (E1) and for the two urea/water mixtures (E4, E5) the linear decay of $\ln(I/I_0)$ versus F is restricted to the first 5–6 min of processing. For pure amorphous urea at 100 K (E2), only the $\delta NH_2 + \nu CO$ band is found to decrease (note that in the photolysis experiments no decay was observed in either band for the comparable sample VUV2). In this case the linear decay in $\ln(I/I_0)$ extends virtually over the whole F range studied.

For the crystalline urea ice ($T = 200$ K) the linear decay of $\ln(I/I_0)$ versus F extends also over all of the F range investigated, in analogy with the behaviour observed in photolysis. The preference for a faster decay of νCN band observed in photolysis is not found in the electron bombardment experiments. In the 30 K urea/water mixture (E4) the νCN band decays indeed faster than the $\delta NH_2 + \nu CO$ band, but the opposite is true for the 100 K mixture (E5) and for the crystalline ice (E3). In the urea/water mixtures, there is a comparatively small decrease in the overall destruction rate of urea with growing temperature, which is in contrast to the behaviour found in the photolysis of urea/water mixtures, where the destruction rate was appreciably smaller for the warmer sample.

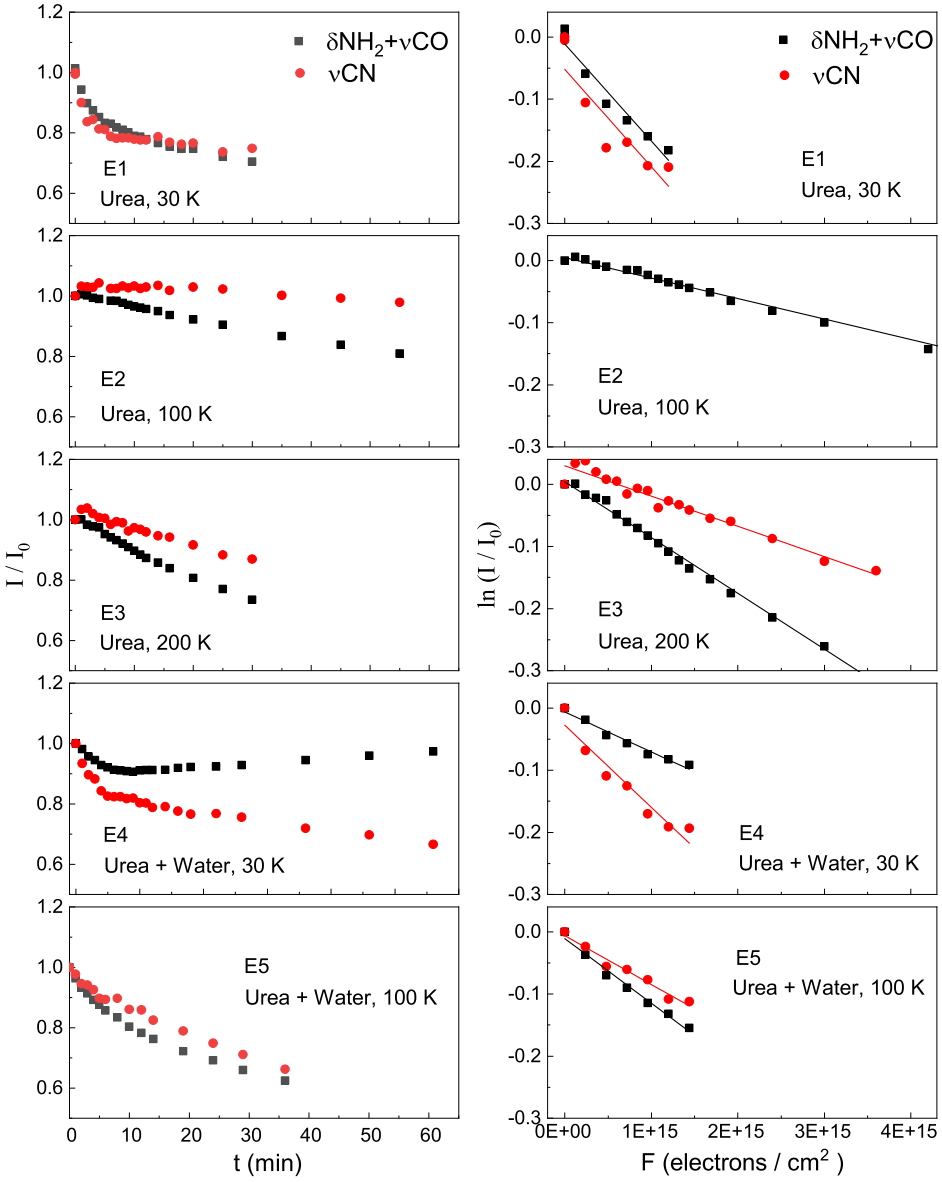

Figure 5. Evolution of the $\delta NH_2 + \nu CO$ (black squares) and νCN (red circles) bands of urea under high-energy (5 keV) electron bombardment. Left-hand column: evolution of the band intensities normalized to the initial value (I/I_0) as a function of time. Right-hand column: fit (straight lines) of the linear decay interval in $\ln(I/I_0)$ to equation (4). The cross-sections derived from the fit are listed in Table 4. The labels E1–E5 correspond to the samples of Table 1.

Table 4. Electron bombardment of urea ices and urea/water ices. Uncertainties (in per cent) are estimated with numerical checks and error propagation in the formulas used to calculate the various quantities in the table. φ_e, electron flux; f_u, molecular fraction of urea (±30 per cent); σ_{des}, destruction cross-section (±20 per cent for pure urea, ±30 per cent for mixtures, fit to equation 4); LET, linear energy transfer (±5 per cent), calculated with the CASINO code (see the text); $D_{1/2}$, half-life dose (±20 per cent for pure urea, ±30 per cent for mixtures, equation 7 or 8); G_{100}, radiation yield (±20 per cent for pure urea, ±30 per cent for mixtures, equation 11 or 12).

Sample	φ_e $\times 10^{12}$ electrons cm^{-2} s^{-1}	σ_{des} $\delta NH_2 + \nu CO$ $\times 10^{-16}$ cm^2	σ_{des} νCN $\times 10^{-16}$ cm^2	LET keV μm^{-1}	$D_{1/2}$ $\delta NH_2 + \nu CO$ eV $molecule^{-1}$	$D_{1/2}$ νCN eV $molecule^{-1}$	G_{100} $\delta NH_2 + \nu CO$ molecules 100 eV^{-1}	G_{100} νCN molecules/100 eV^{-1}
E1 Urea am. $T = 30$ K	4	1.6	1.8	6.9	22	19	3.2	3.6
E2 Urea am. $T = 100$ K	2	0.33	–	6.4	97	–	0.7	–
E3 Urea cry. $T = 200$ K	2	0.90	0.49	6.0	35	64	2.0	1.1
E4 Urea/H_2O $f_u = 0.58$ $T = 30$ K	4	0.64	1.3	5.2	61	32	1.1	2.2
E5 Urea/H_2O $f_u = 0.23$ $T = 100$ K	4	1.0	0.78	4.8	68	87	1.0	0.7

3.3.3 *Energetic yields*

The energetic cost for the destruction of urea ices with UV photons and 5 keV electrons can be estimated with the cross-sections derived in the previous section. We will use to that aim the half-life dose $D_{1/2}$, i.e. the amount of energy needed to reduce by one-half the initial number of urea molecules, and the radiation yield, G, i.e. the number of molecules destroyed upon absorption of a given amount of energy. Usually, this yield is given 'per 100 eV' and is termed G_{100}. In photolysis is also customary to use the quantum yield, Φ_p, which gives the number of molecules destroyed by absorbed photon.

From equation (4), the half-life fluence is defined as

$$F_{1/2} = \ln(2)/\sigma_{des}. \tag{6}$$

The half-life dose can be then calculated as

$$D_{1/2} = \frac{F_{1/2} f_E E}{N_0} = \frac{\ln(2) f_E E}{\sigma_{des} N_0}, \tag{7}$$

where f_E is the fraction of energy deposited by the photons or electrons in the sample, E is the (average) photon or electron energy, and N_0 is the column density at the beginning of the experiment. In the electron bombardment experiments, the energy is deposited in an approximately homogeneous way throughout the sample, and equation (7) can be expressed in terms of the linear energy transfer (LET):

$$D_{1/2} = \frac{\ln(2)\,\mathrm{LET}}{\sigma_{des}\rho}, \tag{8}$$

where ρ is the volume density. For a binary mixture, if the density is not known, it can be roughly approximated by $\rho \approx f_1 \rho_1 + f_2 \rho_2$, where f_i is the fraction of the ith component (see Table 1). The fraction of energy deposited by the electrons and the LET for our experiments were calculated with the CASINO code (Drouin et al. 2007; Drouin 2011). LET values for the samples bombarded with electrons are listed in Table 4.

In the photolysis experiments, the incident radiation can be significantly attenuated within the sample. In this case the absorption of energy is not homogeneous and the optically thin limit ($N \rightarrow 0$) must be taken (Maté et al. 2021). Within this limit,

$$D_{1/2} = \ln(2)\, E \frac{\sigma_a}{\sigma_{des}}, \tag{9}$$

where σ_a is the absorption cross-section. For binary mixtures, the half-life dose of component i becomes (Maté et al. 2021)

$$D_{1/2}(i) = \frac{\ln(2) E}{f_i} \frac{\sigma_a}{\sigma_{des}(i)}, \tag{10}$$

where σ_a is the absorption cross-section of the mixture, and f_i the molecular fraction of component i. If the absorption cross-section of the mixture is not known, it can be roughly approximated by $\sigma_a \approx f_1\sigma_{a1} + f_2\sigma_{a2}$. As indicated above, we are interested in the destruction efficiency at the start of the process when the samples are still largely unprocessed and the presence of secondary products and reverse reactions is minimal. This corresponds to the limit of zero fluence ($F \rightarrow 0$). Under this condition the radiation yield can be expressed as (Maté et al. 2015)

$$G_{100} = 100\, \frac{\sigma_{des} N_0}{E f_E} = 100\, \ln(2)\, D_{1/2}^{-1}. \tag{11}$$

For electron radiolysis, equation (11) can be rewritten in terms of the LET:

$$G_{100} = 100 \frac{\sigma_{des}\rho}{\mathrm{LET}}. \tag{12}$$

For photolysis in the optically thin limit, combining equations (7) and (9)–(11) we obtain

$$G_{100} = 100 \frac{\sigma_{des}}{E_{ph}\sigma_a}, \tag{13}$$

where E_{ph} is the photon energy. Likewise, for the ith component of a binary mixture,

$$G_{100}(i) = 100 \frac{f_i \sigma_{des}(i)}{E_{ph}\sigma_a}, \tag{14}$$

where σ_a is the absorption cross-section of the mixture. The average energy of the photons in our lamp is 8.1 eV (Maté et al. 2018). Using this average photon energy, we can also make a rough estimate of the quantum yield,

$$\Phi_p = \frac{G_{100} E_{ph}}{100} = \frac{\sigma_{des}}{\sigma_a}, \tag{15}$$

and for a binary mixture,

$$\Phi_p(i) = \frac{f_i\, \sigma_{des(i)}}{\sigma_a}. \tag{16}$$

The $D_{1/2}$, G_{100}, and Φ_p obtained for the photolysis and electron radiolysis of the various ices studied in this work are listed in Tables 3 and 4. Radiation yields are small both in photolysis and radiolysis. Overall, the G_{100} values vary between 0.3 and 3.6. The highest values are obtained in the low-temperature (30 K) experiments. For $T \geq 100$ K, radiation yields decrease appreciably and are always smaller than 2. The lower G_{100} values obtained at the higher temperature were unexpected. Intuitively one would expect that an increase in the mobility would lead to a higher destruction rate. We can only speculate that in this case the increase in the mobility with growing T leads to an enhancement of the already mentioned 'repair mechanisms' (energy dissipation or urea recombination). In general, the radiation yields for comparable samples are somewhat larger for electron radiolysis than for VUV photolysis. The estimated photon yields are in the range 10^{-1}–10^{-2}, and in consonance with the G_{100} values, they are higher for the 30 K samples.

The energetic yields for urea destruction shown in Tables 3 and 4 can be compared to previous literature results on the photolysis and radiolysis of the molecule under different circumstances. The UV photolysis of crystalline urea under the conditions of Mars' surface (≈218 K, ≈6 mbar, mostly CO_2) was studied by Poch et al. (2014). They measured the decay of the νCN band under irradiation with 200–250 nm photons from a Xe lamp, and reported photodissociation quantum yields $\Phi_p \approx (1\text{–}1.5) \times 10^{-3}$ molecule photon^{-1} (with a large uncertainty) that are much smaller than those obtained in this work for photolysis with more energetic VUV (120–180 nm) photons. From their measured data (supplementary material, fig. 4), a $\sigma_{des} \approx 10^{-20}$–$10^{-21}$ cm^2 can be deduced, much lower than the VUV destruction cross-sections derived in this study.

γ-ray radiolysis yields, G_{100}, for room temperature crystalline urea ($G_{100} = 0.53$) and for urea in aqueous solutions ($G_{100} = 0.47$) have been reported by Renoult et al. (1969) and by Navarro-González et al. (1989), respectively. The high stability of urea implied by these low G_{100} values is stressed by the authors of these works. They also advance as possible causes an efficient dissipation of the radiation energy within the condensed phases, favoured by an extensive hydrogen bond network, or the rapid recombination of urea from the initially formed radicals, aided by an efficient cage effect. These G_{100} values for γ-ray radiolysis are lower than those obtained in this work for electron bombardment. As discussed above, the mentioned repair mechanisms for urea seem to improve with growing temperature and it is thus possible that they work better at room

Table 5. Lifetimes of urea ice in astrophysical environments.

Environment	Ice lifetime (yr)	VUV dose rate (eV molecule^{-1} yr^{-1})	CR dose rate (eV molecule^{-1} yr^{-1})	Urea VUV half-life (yr)	Urea CR half-life (yr)
Cold dense cloud ($T < 30$ K)	1×10^7	4×10^{-7} [a]	3×10^{-7} [a]	$1.9 \pm 1.5 \times 10^8$	$1.1 \pm 0.9 \times 10^8$
Hot core ($T = 100$ K)	10^4–10^6	4×10^{-7} [a]	3×10^{-7} [a]	$1.3 \pm 1.0 \times 10^9$	$2.4 \pm 1.9 \times 10^9$
KBO (surface) ($T = 30$ K)	4.6×10^9	2.2×10^{-2} [b]	5.6×10^{-3} [c]	$3.5 \pm 2.8 \times 10^3$	$5.7 \pm 4.6 \times 10^3$
KBO 30 μm depth ($T = 30$ K)	4.6×10^9	–	1.6×10^{-8} [d]	–	$2.0 \pm 1.6 \times 10^9$

Note. The VUV half-lives were calculated with urea half-life doses of 77 eV molecule^{-1} (cold dense cloud and Kuiper belt object – KBO) and 552 eV molecule^{-1} (hot core), corresponding to the values given by equation (10) for urea (5 per cent)/water mixtures at 30 and 140 K, respectively (see the text). The cosmic ray (CR) half-lives were calculated with the lowest half-life doses for urea/water mixtures from Table 4, i.e. 32 eV molecule^{-1} (cold dense cloud and KBO) and 72 eV molecule^{-1} (hot core). We have assumed that the VUV and CR dose rates in a hot core are the same as those in a cold dense cloud (Garrod & Vidicus Weaver 2013). [a]Moore et al. (2001) UV doses are estimated for typical ice mantles with a thickness of 20 nm. [b]Moore & Hudson (2005) UV dose rates estimated for the top 15 nm of the ice. [c]Cooper et al. (2003) CR dose rates for ice thickness lower than 10 nm. [d]Strazzula et al. (2003).

temperature than at 100–200 K, which are the highest temperatures studied in this work.

4 ASTROPHYSICAL IMPLICATIONS

As mentioned in the Introduction, urea has been detected at present in diverse astrophysical settings including meteorites (Cooper & Cronin 1995), a hot core (Belloche et al. 2019), and a giant molecular cloud located in the Galactic Centre (Jiménez-Serra et al. 2020), which offer multiple scenarios for urea production and evolution and prompt the investigation of possible formation and destruction pathways. In fact, the molecule has been incorporated into astrochemical models (Belloche et al. 2019), but there are still significant discrepancies between the model results and the observations.

Here we will use the half-life doses derived in the previous section for the estimation of the stability of urea ices towards VUV photons and CRs in different astronomical environments. As indicated previously, we assume that the VUV photons from the D_2 lamp are representative of the secondary VUV field in dense clouds, and also that the effects of 5 keV electrons traversing the ices are comparable to those of MeV protons, that are deemed to be the main components of CRs.

Urea is expected to be at most a minor component in ice mixtures dominated by water and with a significant proportion of CO and CO_2. We have thus taken the half-life doses of the urea–water mixtures for the calculation of the half-lives of urea in space ices. Note, however, that in the mixtures experimentally studied, the proportion of urea is much too high as compared to that expected for astronomical ices. When two half-life doses are available, corresponding to the different decay rates of the $\delta NH_2 + \nu CO$ and νCN bands, we have used the lowest half-life dose, since it gives the lower limit for bond breaking in urea. In the case of photolysis, and assuming as a hypothesis that the main effect of water is the reduction of the average photon flux in the sample (see above), we have estimated the half-life for a 5 per cent proportion of urea in water ice using the experimental cross-sections (Table 3) and equation (10). Estimates of the UV and CR dose rates in different environments are taken from the literature and are indicated, together with their sources, in Table 5. Taking into account the approximations made and the experimental uncertainty of the present measurements, the derived half-lives must be considered as order-of-magnitude estimates.

The half-life doses calculated for urea are listed in the two right-hand columns of Table 5. Urea is found to be very stable against UV radiation and CRs in dense clouds and hot cores. The estimated half-lives are in all cases more than an order of magnitude larger than the expected lifetimes of the ices. The molecule would not survive long (just thousands of years) on the surface of a KBO, due to the large flow of VUV photons and low-energy protons from the solar wind (Cooper et al. 2003), but given the very small penetration depth of these ions in ice, the molecule would be very well protected against CRs at a depth of a few μm below the ice surface. In the case of VUV photolysis, if we assume further that water ice has mainly a protective effect on urea by reducing the photon flux inside the ice, we can use equation (10) to make a rough estimate of the half-life of urea for higher dilutions. Within this approximation, for a 0.1 per cent dilution of urea in water ice, the half-life of urea on the surface of a KBO would increase to $\approx 1.2 \pm 1.0 \times 10^5$ yr, still much less than the lifetime of the Solar system.

In a previous work, we performed a similar study on the stability of 30 K ices of 2-aminooxazole against VUV photons and CRs (Maté et al. 2021). As indicated in the Introduction, this molecule, together with urea, has been proposed as a possible intermediate in a route for the prebiotic synthesis of ribonucleotids. The molecule has been sought, but as yet it has not been found in space. A comparison of the present results with those of Maté et al. (2021) shows that the resistance of urea and 2-aminooxazole to VUV photons and CRs is similar in cold dense clouds and KBOs, with estimated half-lives differing by less than a factor of 1.5 between the two molecules and, thus, this cannot be a cause for the absence of 2-aminooxazole in space. There are however good reasons to expect a lower abundance of 2-aminooxazole as compared with urea. In the first place the bottom-up formation of urea is more likely, given its lower molecular complexity and, besides, in contrast to urea, 2-aminooxazole is easily photodissociated by mid-range UV photons with wavelengths up to 240 nm, which are abundant in the Solar system and are not screened by ice.

A most interesting feature in the energetic processing of urea ices is the appreciable increase in stability observed with growing temperature, which is likely due to efficient repair mechanisms leading to urea reformation. Estimated half-lives for urea in ices at 100 K are an order of magnitude larger than those at 30 K. Results from radiolysis on condensed phases of urea indicate that this stability is even higher at room temperature (Renoult et al. 1969; Navarro-González et al. 1989). Consequently, the molecule should survive the passage from cold dense cloud to hot core in the process of star formation and be available for chemistry over a wide range of conditions in the ensuing protoplanetary disc, being thus a good candidate for prebiotic syntheses.

5 SUMMARY AND CONCLUSIONS

Motivated by the recent detection of urea in the ISM and by the possible key role of this molecule in prebiotic chemical syntheses, we have investigated the stability of urea and urea/water ice mixtures subjected to VUV (120–180 nm) irradiation and high-energy (5 keV) electron bombardment under conditions relevant for the ISM and outer Solar system bodies. The effects of irradiation were followed *in situ* by means of IR spectroscopy. The main findings of this work are listed here.

(1) The energetic processing of ice samples led to the destruction of urea and to the formation of new species. The only new products clearly identified were CO_2, HNCO, and OCN^- that were observed, both in photolysis and in electron radiolysis. The three species were found in the experiments performed at 30 K, and OCN^- was found in all the experiments. For $T \geq 100$ K, CO_2 and HNCO virtually disappeared. Other products with IR absorption bands coincident with those of urea cannot be excluded. Appreciable amounts of species with high molecular weight were not formed since no residues remained after heating the sample substrates at 300 K.

(2) In the photolysis experiments, the largest cross-sections for urea destruction ($\approx$3–6 $\times$ 10^{-18} cm^{-2}) were found for amorphous samples at 30 K. Significantly smaller destruction cross-sections ($\approx$1–1.5 $\times$ 10^{-18} cm^{-2}) were found for amorphous ice deposits at 100–140 K and for crystalline urea at 200 K. In the urea/water ice mixtures, water molecules absorb part of the photons, but do not seem to participate directly in the urea chemistry. Estimated quantum yields for urea destruction are in the 2–0.2 $\times$ 10^{-2} molecules photon^{-1} interval.

(3) In the electron radiolysis measurements, the largest destruction cross-sections were also found at 30 K ($\approx$1.3–1.8 $\times$ 10^{-16} cm^{-2}), and a decrease of the destruction cross-section with temperature was also observed for the samples of pure urea at 100 and 200 K.

(4) Radiation yields for urea destruction were comparatively small (G_{100} = 3.6–0.3 molecules/100 eV), both for photolysis and radiolysis. Electron bombardment was found to be somewhat more efficient than VUV photolysis for the destruction of urea molecules. The stability of urea and urea/water ices increases (the G_{100} values decrease) with growing temperature pointing to the presence of efficient repair mechanisms, either due to energy dissipation or urea reformation, that are enhanced with increasing mobility.

(5) Estimates based on the present laboratory data show that urea ices should be very stable against VUV radiation and CRs in cold dense clouds and even more in hot cores. They would be easily destroyed on top of the surface of KBOs, due to the intense VUV field and to the large flux of slow protons from the solar wind, but would survive under just a few microns of ice. The stability of urea ices increases with growing temperature, which indicates that the molecule, once formed, should be available over a wide range of physical conditions and makes it a good candidate for prebiotic chemistry both in the Earth and in outer space.

ACKNOWLEDGEMENTS

BM, IT, and VJH acknowledge support from the Ministerio de Economia y Competitividad (MINECO) and the Ministerio de Ciencia e Innovación (MICINN) of Spain under grants FIS2016-77726-C3-1-P and PID2020-113084GB-100 and from the European Union under grant ERC-2013-Syg-210656-NANOCOSMOS. GMMC and HC are grateful for funding from MICINN under grant PID2020-118974GB-C21, and PhD fellowship FPU-17/03172. IJ-S acknowledges financial support from grant N^{o} PID2019-105552RB-C41 by the Spanish Ministry of Science and Innovation/State Agency of Research MCIN/AEI/10.13039/501100011033. GMMC, HC, and IJ-S also acknowledge support from MDM-2017–0737 Unidad de Excelencia 'María de Maeztu' – CAB (CSIC-INTA). The i-LINK program (grant LINKA 20353) from CSIC is also acknowledged.

DATA AVAILABILITY

All the data supporting this research are available in the paper.

REFERENCES

Arumainayagam C. R. et al. 2019, Chem. Soc. Rev., 49, 2293
Becker S. et al. 2019, Science, 366, 6461
Belloche A., Garrod R. T., Müller H. S. P., Menten M. K., Medvedev I., Thomas J., Kisiel Z., 2019, A&A, 628, A10
Campbell B. F., Clark L. B., 1989, J. Am. Chem. Soc., 111, 8131
Chyba C., Sagan C., 1992, Nature, 355, 125
Cooper G. W., Cronin J. R., 1995, Geochim. Cosmochim. Acta, 59, 1003
Cooper J. F., Christian E. R., Richardson J. D., Wang C. H., 2003, Earth Moon Planets, 92, 261
Cruz-Díaz G. A., Muñoz-Caro G. M., Chen Y.-J., Yih T.-S., 2014, A&A, 562, A119
Dohnhálek Z., Kimmel G. A., Ayotte P., Smith R. S., Kay B. D., 2003, J. Chem. Phys., 118, 364
Drouin D., 2011, CASINO: Monte Carlo Simulation of Electron Trajectory in Solids. http://www.gel.usherbrooke.ca/casino
Drouin D., Couture A. R., Joly D., Tastet X., Aimez V., Gauvin R., 2007, Scanning, 29, 92
Duvernay F., Chiavassa T., Borget F., Aycard J. P., 2005, J. Phys. Chem. A, 109, 6008
Gálvez Ó., Maté B., Herrero V. J., Escribano R., 2010, ApJ, 724, 539
Garrod R. T., Vidicus Weaver S. L., 2013, Chem. Rev., 113, 8939
Hayatsu R., Studier M. H., Moore L. P., Anders E., 1975, Geochim. Cosmochim. Acta, 39, 471
Hudson R. L., 2018, Phys. Chem. Chem. Phys., 20, 5389
Jiménez-Serra I. et al., 2020, Astrobiology, 20, 1048
Kaiser R. I., Stockton A. M., Kim Y. S., Jensen E. C., Mathies R. A., 2013, ApJ, 765, 111
Lowenthal M. S., Kahnna R. K., Moore M. H., 2002, Spectrochim. Acta A: Mol. Biomol. Spectrosc., 58, 73
Mason N. J., Nair B., Jheeta S., Shymańska E., 2014, Faraday Discussions, 168, 235
Mastrapa R. M., Sandford S. A., Roush T. L., Cruikshank D. P., Dalle Ore C. M., 2009, ApJ, 701, 1347
Maté B., Gálvez Ó., Herrero V. J., Fernández-Torre D., Moreno M. A., Escribano R., 2009, ApJ, 703, L178
Maté B., Rodríguez-Lazcano Y., Gálvez O., Tanarro I., Escribano R., 2011, Phys. Chem. Chem. Phys., 13, 12268
Maté B., Tanarro I., Moreno M. A., Jiménez-Redondo M., Escribano R., Herrero V. J., 2014, Faraday Discussions, 168, 267
Maté B., Tanarro I., Escribano R., Moreno M. A., Herrero V. J., 2015, ApJ, 806, 151
Maté B., Molpeceres G., Jiménez-Redondo M., Tanarro I., Herrero V. J., 2016, ApJ, 831, 51
Maté B., Molpeceres G., Tanarro I., Peláez R. J., Guillemin J. C., Cernicharo J., Herrero V. J., 2018, ApJ, 861, 61
Maté B. et al., 2021, ApJ, 909, 123
Menor-Salván C., Marín-Yaseli M. R., 2012, Chem. Soc. Rev., 41, 5404
Menor-Salván C., Bouza M., Fialho D. M., Burcar B. T., Fernández F. M., Hud N. V., 2020, ChemBioChem, 21, 3504

Moore M. H., Hudson R. L., 2005, in Lis D. C., Blake G. S., Herbst E., eds, Proc. IAU Symp. 231, Astrochemistry: Recent Success and Current Challenges. Cambridge Univ. Press, Cambridge, p. 247
Moore M. H., Hudson R. L., Gerakines P. A., 2001, Spectrochim. Acta A: Mol. Biomol. Spectrosc., 57, 843
Muñoz-Caro G. M., Jiménez-Escobar A., Martín-Gago J. Á., Rogero C., Atienza C., Puertas S., Sobrado J. M., Torres-Redondo J., 2010, A&A, 522, A108
Navarro-González R., Negrón-Mendoza A., Chacón E., 1989, Origins Life Evolution Biosphere, 19, 109
Patel B. H., Percivalle C., Ritson D. J., Duffy C. D., Sutherland J. D., 2015, Nat. Chem., 7, 301
Peeters Z., Hudson R. L., Moore M. H., Lewis A., 2010, Icarus, 210, 480
Poch O., Kaci S., Stalport F., Szopa C., Coll P., 2014, Icarus, 242, 50
Powner M. W., Gerland B., Sutherland J. D., 2009, Nature, 459, 239
Renoult D. H., McCallum K. J., Woods R. J., 1969, Int. J. Radiat. Phys. Chem., 1, 495
Strazzula G., Cooper J. F., Christian E. R., Johnson R. E., 2003, Comptes Rendus - Phys., 4, 791
Terasaki M., Nomoto S., Mita H., Shimoyama A., 2002, Origins Life Evolution Biosphere, 32, 91
Timón V., Maté B., Herrero V. J., Tanarro I., 2021, Phys. Chem. Chem. Phys., 23, 22344
Van Broekhuizen F. A., Keane J. V., Shutte W. A., 2004, A&A, 415, 425

This paper has been typeset from a TEX/LATEX file prepared by the author.